Korean J. Chem. Eng., 40(12), 3046-3051 (2023)
DOI: 10.1007/s11814-023-1526-8

pISSN: 0256-1115
eISSN: 1975-7220

Effect of hierarchically reduced SiO_x on anode performance of Li-ion batteries

Dan-Bi Moon‡, Kue-Ho Kim‡, and Hyo-Jin Ahn†

Department of Materials Science and Engineering, Seoul National University of Science and Technology, Seoul 01811, Korea
(*Received 29 May 2023 • Revised 23 June 2023 • Accepted 29 June 2023*)

Abstract−Renewable energy sources have attracted considerable attention in both academia and industry owing to concerns about environmental pollution, global warming, and fossil fuel depletion. In this regard, the application scope of Li-ion batteries (LIBs) is continuously broadening owing to their advantages, such as their high energy and power densities, eco-friendliness, and portability. As highly capacitive anode materials for LIBs, Si-based materials should circumvent the critical limitations of large volume expansion and low electrical conductivity. Herein, we propose hierarchically reduced SiO_x as an anode material for LIBs. Using the magnesiothermic reduction process, we optimized the electrical conductivity and kinetic properties of SiO_x materials based on SiO_2. The resultant SiO_x electrode exhibited a high specific capacity of 1,286.8 mAh g^{-1} along with stable cyclability up to 100 cycles. The enhanced electrochemical performance was mainly attributed to the oxygen vacancies and mesoporous surface morphology of SiO_x, which were generated during hierarchical magnesiothermic reduction. This study demonstrates the correlation between the structural properties and electrochemical performance according to the reduction level of Si-based active materials.

Keywords: Li-ion Batteries, Anodes, Silicon Suboxides, Reduction, Oxygen Vacancy

INTRODUCTION

Owing to the development of state-of-the-art electronic devices with various functions, the demand for high-performance portable energy-storage devices has increased significantly, expanding their global market [1-4]. Moreover, concerns about environmental pollution, global warming, and fossil fuel depletion have increased the demand for renewable energy sources. The applications of Li-ion batteries (LIBs) have broadened, encompassing most energy-storage media (from small to large scale) in electronic devices. The performance of LIBs is determined by factors such as energy density, power density, cyclability, and stability [5,6]. To enhance these factors, it is important to control the electrochemical reactions inside the unit cell during the charge/discharge processes. Generally, LIBs consist of four main functional layers: the anode, cathode, separator, and electrolyte. The separator prevents short circuits by dividing the electrodes, and the electrolyte functions as an ion shuttle through the ionic pathway. The anode and cathode, as the main parts of the electrochemical reaction, perform the actual energy storage function and dominantly affect the performance of LIBs [7]. In the LIBs, the anode charges the electrochemical energy through the reaction between the Li-ion and anode materials such as graphite and silicon.

Graphite has been adopted as a representative anode material owing to its several advantages, such as its low cost and high stability. However, to develop advanced LIBs with high energy-storage capacity, the poor theoretical capacity of graphite (~372 mA h g^{-1}) should be resolved [8]. This limitation was circumvented using Si-based anode materials, which have an excellent theoretical capacity (~4,200 mA h g^{-1}) compared with other reported anode materials and a low working potential (<0.5 V, vs. Li/Li^+), making them promising for next-generation LIBs [9]. However, pure Si anode materials commonly exhibit poor cycling performance owing to the large volume expansion (400%) during the lithiation and delithiation processes. As an alternative, SiO_2 has been investigated. It has a high theoretical capacity (~1,965 mA h g^{-1}) owing to its alleviated volume expansion rate; however, it also has a critical disadvantage of low electrical conductivity [10-12]. Because of its poor electrical characteristics, SiO_2 is generally adopted in composites with highly conductive materials. Despite the high theoretical capacity of Si-based anode materials, the aforementioned limitations significantly hinder the commercialization of Si-based anodes with high energy density. To overcome the disadvantages of Si-based anode materials, the construction of a hybrid composite structure is an effective strategy to increase electrical conductivity [13,14]. However, this strategy cannot solve the intrinsic problems of Si-based materials, and it is difficult to optimize their composition. In another approach, the partial reduction of oxide materials can ameliorate their electrical properties, enhancing their electrochemical performance. Recently, reduced silicon suboxides (SiO_x) have attracted considerable attention owing to their modifiable physical and electrochemical properties. The reduction of SiO_2 to SiO_x, and the morphological and structural effects of the reduction process on the electrochemical performance, have not yet been widely studied. Among the various reduction techniques for oxide materials, the magnesiothermic reduction process has several advantages, including low cost, high reactivity, and high productivity. Moreover, the etching process of MgO after magnesiothermic reaction can provide a porous structure, which can contribute to the electrochemical performances.

In this study, we prepared hierarchically reduced SiO_x (SiO_x-1.5 Mg, SiO_x-2.5 Mg, SiO_x-3.5 Mg, and SiO_x-4.5 Mg) via magnesiother-

†To whom correspondence should be addressed.
E-mail: hjahn@seoultech.ac.kr
‡D.-B. Moon and K.-H. Kim contributed equally to this work.

mic reduction from SiO_2 powder to verify the morphological and structural variations according to the reduction level. During the magnesiothermic process, oxygen vacancies were generated, providing additional charge carriers for SiO_x. Moreover, the removal of the MgO particles after heat treatment induced a mesoporous surface morphology in SiO_x. The physical and chemical characteristics were analyzed in detail by optimizing the reduction level of SiO_2, which led to the optimization of the electrochemical performance. The resultant anode using the SiO_x-3.5 Mg sample exhibited the highest electrical conductivity and ionic diffusivity with the highest cyclability, owing to the optimized reduction level and mesoporous surface morphology.

EXPERIMENTAL DETAILS

Hierarchically reduced SiO_x samples were fabricated via magnesiothermic reduction. Untreated bare SiO_2 (>99%, Sigma-Aldrich) was homogeneously blended with Mg (>99%, Sigma-Aldrich) to induce a uniform magnesiothermic reaction. To adjust the reduction level of SiO_2, the SiO_2 : Mg molar ratio was set as 1 : 1.5, 1 : 2.5, 1 : 3.5, and 1 : 4.5; the corresponding samples are denoted as SiO_x-1.5 Mg, SiO_x-2.5 Mg, SiO_x-3.5 Mg, and SiO_x-4.5 Mg, respectively. After the mixing process, the blended powder was heated to 670 °C for 2 h under an N_2 atmosphere in a tube furnace for hierarchically reducing SiO_2 to SiO_x according to the Mg amount. During the heat treatment, Mg was oxidized to MgO as a result of the magnesiothermic reaction. To remove MgO and the reaction residue, SiO_x was cleaned repeatedly with a hydrochloric acid (~37%, Samchun) solution and deionized water. The resultant powders were dried in an oven at 80 °C for 12 h to obtain a brown SiO_x powder.

The surface morphologies of the fabricated samples were analyzed using high-resolution field-emission scanning electron microscopy (FESEM; Hitachi SU8010). To investigate the crystallographic and chemical bonding structures and the component ratios of the synthesized samples, X-ray diffraction (XRD; X'Pert Pro) and X-ray photoelectron spectroscopy (XPS; K-Alpha$^+$) analyses were performed. To evaluate the electrochemical performance, coin cells (Hohsen, CR2032) were assembled using the synthesized SiO_x anode, Li metal with a thickness of 1T (Honjo Chemical), 1.6 M $LiPF_6$ in a DEC : EC (3 : 7) solvent as an electrolyte, and a polyethylene separator. The slurries for the anode were fabricated using the synthesized SiO_x samples as the active materials, Super P as the conductive material, and polyacrylic acid as the binder at a 7 : 1 : 2 ratio. The active material loading masses of the respective electrodes were maintained at approximately 1.2 mg to minimize errors during the measurement of electrochemical characteristics. Electrochemical impedance spectroscopy (EIS) was performed in the range of 10^5 to 10^{-2} Hz to evaluate the electrical conductivity and electrochemical kinetic properties of the electrodes. A battery charge/discharge cycler (WonATech, WBCS 3,000 L) was used to evaluate the energy-storage performance in the potential range of 0.05-1.50 V (vs. Li/Li$^+$). The cycle stability was analyzed for 100 cycles at a current density of 1,000 mA g^{-1}.

RESULTS AND DISCUSSION

Hierarchically reduced SiO_x samples were prepared via magnesiothermic reduction of SiO_2 powder. Fig. 1 shows an image of the fabrication process, including the magnesiothermic process and further etching steps. Untreated SiO_2 powder was blended with various amounts of Mg, with ratios of SiO_2 : Mg as 1 : 1.5, 1 : 2.5, 1 : 3.5, and 1 : 4.5, to control the reduction level of SiO_x. For the magnesiothermic process, uniformly blended powder was heat-treated up to 670 °C for 2 h under an N_2 atmosphere. During the heat treatment, the blended powder underwent the following chemical reactions owing to thermal energy [15]:

$$SiO_2+4Mg \rightarrow Mg_2Si+2MgO \quad (1)$$

$$Mg_2Si+SiO_2 \rightarrow 2Si+2MgO. \quad (2)$$

Above 300 °C, SiO_2 reacted with Mg, forming Mg_2Si and MgO phases. As the temperature reached 600 °C, the generated Mg_2Si and residual SiO_2 formed Si and MgO phases [16]. Consequently, the SiO_2 was reduced to SiO_x, accompanied by the generation of MgO (oxidation of Mg). After the heat treatment, the generated MgO particles were removed via HCl etching, resulting in a mesoporous surface morphology owing to the vacant MgO sites.

Fig. 2 shows FESEM images of bare SiO_2, SiO_x-1.5 Mg, SiO_x-2.5 Mg, SiO_x-3.5 Mg, and SiO_x-4.5 Mg; digital photographs of the powders are presented in the insets. All the samples exhibited microscale particle sizes in the range of 1.2-1.8 μm. As shown in Fig. 2(a), the bare SiO_2 sample, which was obtained before magnesiothermic reduction, had a smooth surface and a white color. As the reduction level of the samples increased from SiO_x-1.5 Mg to SiO_x-4.5 Mg, the colors of the powders became darker owing to the band-gap narrowing (Figs. 2(b)-(e)) [17]. From SiO_2 to SiO_x and Si, the

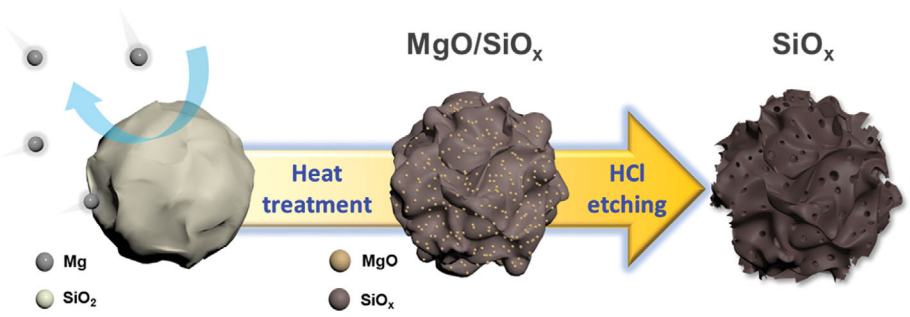

Fig. 1. Fabrication of SiO_x samples from SiO_2 powder.

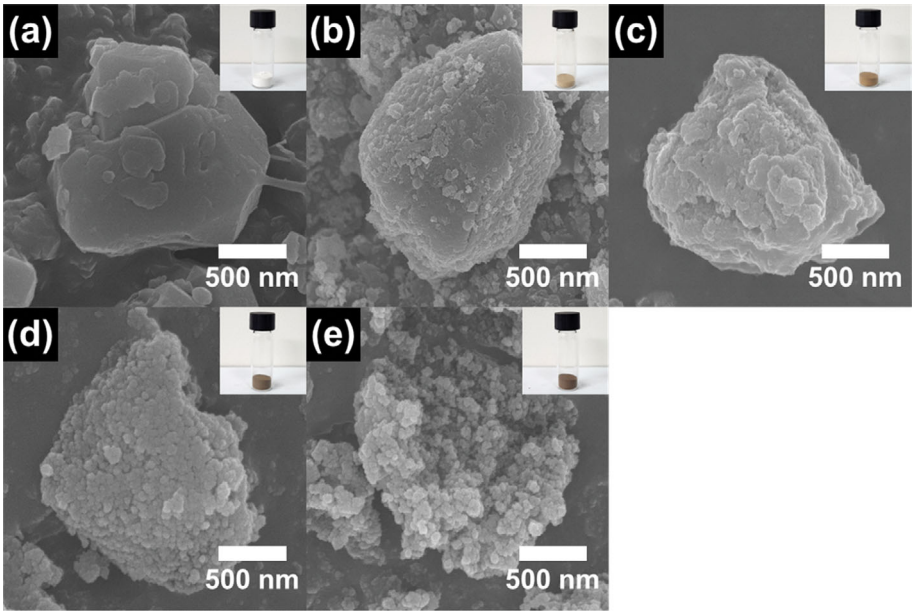

Fig. 2. FESEM images and digital photographs of the (a) SiO_2, (b) SiO_x-1.5 Mg, (c) SiO_x-2.5 Mg, (d) SiO_x-3.5 Mg, and (e) SiO_x-4.5 Mg samples.

electrical conductivity increased owing to the generation of oxygen vacancies together with additional charge carriers, which endowed the Si-based materials with metallic properties. Moreover, the increased Mg content led to the development of a large MgO phase, which contributed to the mesoporous surface morphology of the SiO_x samples. However, for SiO_x-4.5 Mg, an excess Mg amount resulted in a smashed particle morphology because of the large amount of MgO, which was removed by HCl etching. The cracked and damaged particle morphology of SiO_x-4.5 Mg can even induce an irreversible redox reaction by forming an excessive amount of solid-electrolyte interphase (SEI). Thus, the SiO_x-3.5 Mg sample exhibited an optimized particle morphology with a mesoporous surface, while maintaining a solid particle state.

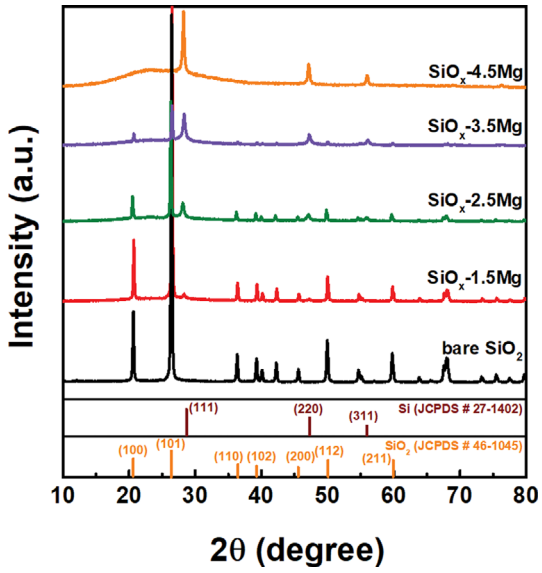

Fig. 3. XRD data obtained from the SiO_2, SiO_x-1.5 Mg, SiO_x-2.5 Mg, SiO_x-3.5 Mg, and SiO_x-4.5 Mg samples.

Fig. 3 shows the XRD patterns of bare SiO_2, SiO_x-1.5 Mg, SiO_x-2.5 Mg, SiO_x-3.5 Mg, and SiO_x-4.5 Mg, which were obtained to identify the crystal structures. The bare SiO_2 sample exhibits typical crystalline SiO_2 peaks at approximately 20.6°, 26.4°, 36.4°, 39.3°, 45.6°, 50.1°, and 59.9°, corresponding to the (100), (101), (110), (102), (200), (112), and (211) planes of SiO_2, respectively (JCPDS #46-1045) [18]. Interestingly, as the reduction level of SiO_x increased from SiO_x-1.5 Mg to SiO_x-4.5 Mg according to the amount of Mg added, the intensities of the SiO_2 peaks decreased, and Si peaks emerged. For the SiO_x-4.5 Mg sample, only Si peaks were observed at approximately 28.7°, 47.3°, and 55.9°, corresponding to the (111), (220), and (311) planes of Si, respectively (JCPDS #27-1402). This indicates that hierarchically reduced SiO_x samples were successfully prepared by adjusting the amount of Mg relative to that of SiO_2.

XPS analyses of the SiO_x-1.5 Mg, SiO_x-2.5 Mg, SiO_x-3.5 Mg, and SiO_x-4.5 Mg samples were conducted to determine the chemical bonding states and oxidation numbers. Fig. 4(a) shows the O 1s XPS profiles obtained from the samples, which were standardized with the C-C (284.5 eV) reference binding energy. All the samples exhibited two peaks at approximately 534.0 and 533.3 eV, corresponding to the O-Si(I) and O-Si(II) bonds of silicon oxide, respectively [19]. As the reduction level increased from SiO_x-1.5 Mg to SiO_x-4.5 Mg, the O 1s peak intensity decreased because of the magnesiothermic reduction process. Notably, the intensity of the oxygen vacancy peak at approximately 529 eV increased with the amount of Mg. These oxygen vacancies introduce additional charge carriers to the SiO_x lattice, increasing the electrical conductivity [20,21]. Low electrical conductivity is a critical limitation of Si-based active materials, as it restricts the formation of an SEI layer and disrupts electron transport during the charge and discharge processes. Thus, the generation of oxygen vacancies in the SiO_x active material can significantly improve the electrochemical performance. Using the XPS data, the peak area ratios (Si/O) and detailed oxidation num-

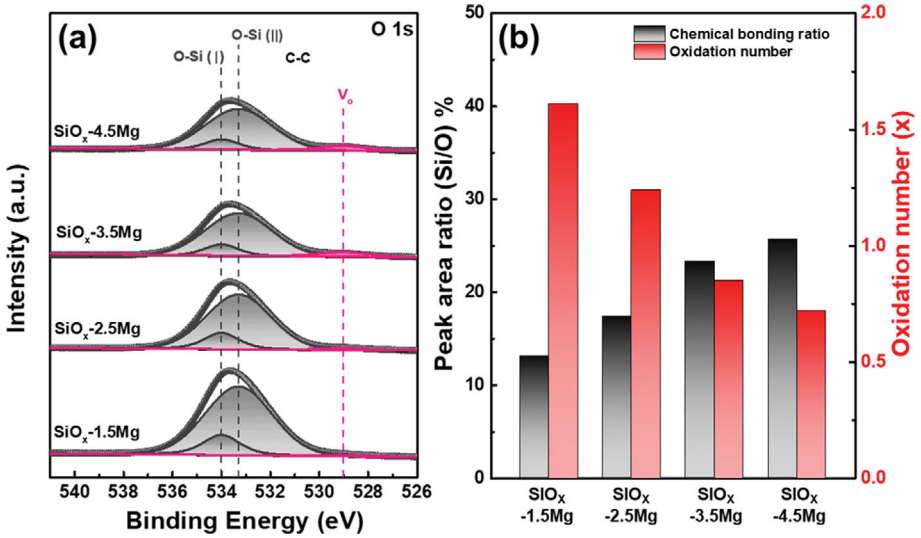

Fig. 4. (a) O 1s XPS core-level spectra and (b) calculated peak area ratios based on the oxidation numbers for the SiO_x-1.5 Mg, SiO_x-2.5 Mg, SiO_x-3.5 Mg, and SiO_x-4.5 Mg samples.

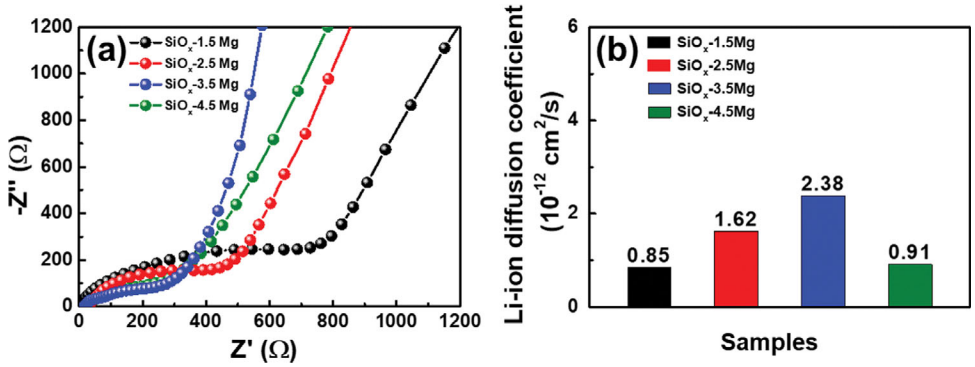

Fig. 5. (a) Nyquist plots and (b) calculated Li-ion diffusion coefficients of the SiO_x-1.5 Mg, SiO_x-2.5 Mg, SiO_x-3.5 Mg, and SiO_x-4.5 Mg electrodes.

bers of the SiO_x-1.5 Mg, SiO_x-2.5 Mg, SiO_x-3.5 Mg, and SiO_x-4.5 Mg samples were calculated. The peak area ratios (Si/O) for SiO_x-1.5, SiO_x-2.5 Mg, SiO_x-3.5 Mg, and SiO_x-4.5 Mg were 13.1%, 17.4%, 23.3%, and 25.7%, respectively. The calculated oxidation numbers for SiO_x-1.5 Mg, SiO_x-2.5 Mg, SiO_x-3.5 Mg, and SiO_x-4.5 Mg were 1.61, 1.24, 0.85, and 0.72, respectively. The results indicate that the oxidation numbers of the SiO_x samples were easily controlled through the magnesiothermic reduction process. Moreover, the oxygen vacancies in the optimized SiO_x sample affected its electrochemical performance.

To investigate the electrochemical kinetic properties of the SiO_x-1.5 Mg, SiO_x-2.5 Mg, SiO_x-3.5 Mg, and SiO_x-4.5 Mg anodes, EIS was conducted using coin-type cells. Fig. 5(a) shows the Nyquist plots, which are often divided into semicircles and inclined lines in the high- and low-frequency regions, respectively. The semicircle indicates the charge-transfer resistance (R_{ct}), which corresponds to the interfacial resistance between the anode and electrolyte. Among the electrodes, the SiO_x-3.5 Mg electrode exhibits the smallest semicircle, indicating that it has the highest electrical conductivity. This result is mainly attributed to the optimized reduction level of SiO_x with the generated oxygen vacancies. The inclined line is related to Li-ion diffusivity, which is expressed by the Warburg impedance. The SiO_x-3.5 Mg electrode exhibits the lowest Warburg impedance, resulting from the enhanced Li-ion diffusivity due to the mesoporous surface morphology. Fig. 5(b) shows the Li-ion diffusion coefficients based on the Warburg impedance coefficients (σ_w), which were obtained from the slopes of all the electrodes. To calculate the Li-ion diffusion coefficient, we utilized a relevant equation as below:

$$D=(RT)^2/2A(n^2F^2C\sigma_w)^2 \quad (3)$$

First, to get the ionic diffusion coefficient (D), the Warburg impedance coefficients (σ_w) were obtained from the slope of Nyquist plot of respective samples. The values of σ_w were exhibited as 19.9, 14.5, 12.0, and 19.3 for SiO_x-1.5 Mg, SiO_x-2.5 Mg, SiO_x-3.5 Mg, and SiO_x-4.5 Mg electrodes, respectively. Based on these values, the SiO_x-3.5 Mg electrode exhibits the largest Li-ion diffusion coefficient (2.38×10^{-12} cm^2 s^{-1}) among the electrodes (0.85×10^{-12}, 1.62×10^{-12}, and 0.91×10^{-12} cm^2 s^{-1} for SiO_x-1.5 Mg, SiO_x-2.5 Mg, and SiO_x-4.5 Mg, respectively).

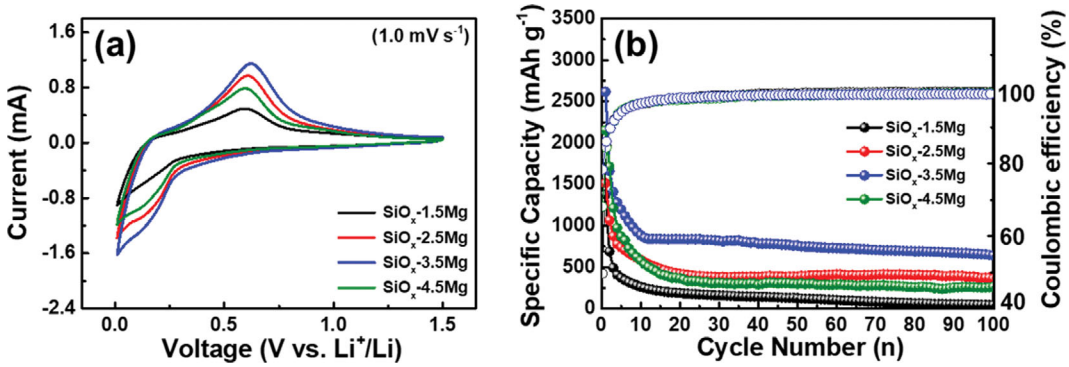

Fig. 6. (a) CV data measured from 0.05 to 1.5 V at a scan rate of 1.0 mV s^{-1} and (b) specific capacities at a current density of 0.5C for the SiO_x-1.5 Mg, SiO_x-2.5 Mg, SiO_x-3.5 Mg, and SiO_x-4.5 Mg electrodes.

The cyclic voltammetry (CV) curves of the electrodes obtained at a scan rate of 1.0 mV s^{-1} were plotted to evaluate the electrochemical characteristics with respect to the voltage, as shown in Fig. 6(a). All the electrodes exhibit a pair of anodic and cathodic peaks at approximately 0.59 and 0.016 V, corresponding to the lithiation and delithiation processes, respectively, during the repeated redox reactions [22]. The SiO_x-3.5 Mg electrode exhibits the highest anodic and cathodic peak current densities among the electrodes, which is mainly attributed to its high electrical conductivity and facilitated diffusion. To evaluate the energy-storage capabilities of the electrodes, repeated charge and discharge tests were performed for 100 cycles at a current density of 0.5C. In addition, the charge and discharge initial Coulombic efficiencies (ICEs) were calculated (Fig. 6(b)). The ICE values of the samples appeared as 49.62%, 57.29%, 78.36%, and 68.18% for SiO_x-1.5 Mg, SiO_x-2.5 Mg, SiO_x-3.5 Mg, and SiO_x-4.5 Mg, respectively. The SiO_x-4.5 Mg exhibits a reduced ICE despite having the lowest oxygen content; this is attributed to the cracked and unstable particle morphology. Owing to its high electrical conductivity and mesoporous surface morphology, the SiO_x-3.5 Mg electrode exhibits the highest specific capacity (1,286.8 mAh g^{-1}) and cycle stability for 100 cycles (658.1 mAh g^{-1} at the 100^{th} cycle) among the electrodes. This result indicates the effect of the hierarchical reduction process of SiO_x on its electrochemical performance. For the SiO_x-4.5 Mg electrode, excessive magnesiothermic reduction destroyed the particle structure and degraded the electrochemical performance.

The electrochemical performance of hierarchically reduced SiO_x was successfully optimized using magnesiothermic reduction. During heat treatment, Mg reacted with SiO_2, reducing SiO_2 to SiO_x and Si with the generation of MgO. The oxygen vacancies and metallic Si structure increased the electrical conductivity of SiO_2, accelerating electron transport during the redox reaction. Furthermore, the etched MgO sites formed a mesoporous surface morphology, which improved the cycle stability. According to these results, hierarchically reduced SiO_x is a promising anode material for high-performance LIBs.

CONCLUSION

The effects of the hierarchical reduction of SiO_x on the energy-storage capabilities of LIB anodes were investigated. We controlled the reduction of SiO_x from bare SiO_2 via a magnesiothermic process. SiO_x-3.5 Mg had a larger number of oxygen vacancies and a more mesoporous surface morphology than the other samples. The SiO_x-3.5 Mg electrode exhibited the largest Li-ion diffusion coefficient (2.38×10^{-12} cm^2 s^{-1}) and the highest specific capacity (1,286.8 mAh g^{-1}). These performance enhancements were affected by the following factors: (1) The optimized reduction process increased the electrical conductivity owing to the Si metallic phase with additional charge carriers from oxygen vacancies. The high electrical conductivity facilitated electron transport during the charge and discharge processes, which contributed to a high specific capacity. (2) A well-developed mesoporous surface morphology resulting from the removal of MgO enhanced the cycle stability. Therefore, the SiO_x-3.5 Mg electrodes are an attractive substitute for conventional anode materials used in LIBs.

ACKNOWLEDGEMENTS

This study was supported by a Research Program funded by SeoulTech (Seoul National University of Science and Technology).

CONFLICTS OF INTEREST

The authors declare no conflicts of interest.

REFERENCES

1. X. Han, W. Zhou, M. Chen, J. Chen, G. Wang, B. Liu, L. Luo, S. Chen, Q. Zhang, S. Shi and C.-P. Wong, *J. Energy Chem.*, **67**, 727 (2022).
2. Y. Qi, G. Wang, S. Li, T. Liu, J. Qiu and H. Li, *Chem. Eng. J.*, **397**, 125380 (2020).
3. Y. Yang, E. G. Okonkwo, G. Huang, S. Xu, W. Sun and Y. He, *Energy Storage Mater.*, **36**, 186 (2021).
4. C. Lv, X. Zhou, L. Zhang, C. Yan, M. Srinivasan, Z. W. She, C. Liu, H. Pan, S. Li, Y. Wen and Q. Yan, *Adv. Mater.*, **34**, 2101474 (2022).
5. M. Zhang, Y. Liu, D. Li, X. Cui, L. Wang, L. Li and K. Wang, *Energies*, **16**, 1599 (2023).
6. Z. Li, Y. Zhang, T. Liu, X. Gao, S. Li, M. Ling, C. Liang, J. Zheng

and Z. Lin, *Adv. Energy Mater.*, **10**, 1903110 (2020).
7. K.-H. Kim, T.-J. Song and H.-J. Ahn, *Appl. Surf. Sci.*, **608**, 155084 (2023).
8. P. Li, H. Kim, S.-T. Myung and Y.-K. Sun, *Energy Storage Mater.*, **35**, 550 (2021).
9. S. Chae, S.-H. Choi, N. Kim, J. Sung and J. Cho, *Angew. Chem.-Int. Edit.*, **59**, 110 (2020).
10. D. Sui, M. Yao, L. Si, K. Yan, J. Shi, J. Wang, C. C. Xu and Y. Zhang, *Carbon*, **205**, 510 (2023).
11. T. Liu, Y. Qu, J. Liu, L. Zhang, B. Cheng and J. Yu, *Small*, **17**, 2103673 (2021).
12. W. Wu, M. Wang, J. Wang, C. Wang and Y. Deng, *ACS Appl. Energy Mater.*, **3**, 3884 (2020).
13. Q. Chen, L. Tan, S. Wang, B. Liu, Q. Peng, H. Luo, P. Jiang, H. Tang and T. Sun, *Electrochim. Acta*, **385**, 138385 (2021).
14. H. Jin, M. Zhu, J. Liu, L. Gan, Z. Gong and M. Long, *Appl. Surf. Sci.*, **541**, 148436 (2021).
15. J. Tang, L. Hou, T. Hu, S. Fan, X. Zhou and J. Yang, *Compos. Commun.*, **23**, 100544 (2021).
16. J. Zhang, S. Zuo, Y. Wang, H. Yin, Z. Wang and J. Wang, *J. Power Sources*, **495**, 229803 (2021).
17. S. B. Patil, H. Phattepur, B. Kishore, R. Viswanatha and G. Nagaraju, *Mater. Renew. Sustain. Energy*, **8**, 10 (2019).
18. B. Hariyanto, D. A. P. Wardani, N. Kurniawati, N. P. Har, N. Darmawan and Irzaman, *J. Phys.*, **2019**, 012106 (2021).
19. H.-P. Ma, J.-H. Yang, J.-G. Yang, L.-Y. Zhu, W. Huang, G.-J. Yuan, J.-J. Feng, T.-C. Jen and H.-L. Lu, *Nanomaterials*, **9**, 55 (2019).
20. K.-H. Kim, B.-R. Koo and H.-J. Ahn, *Ceram. Int.*, **44**, 9408 (2018).
21. B.-R. Koo, D.-H. Oh and H.-J. Ahn, *Appl. Surf. Sci.*, **433**, 27 (2018).
22. H. Xue, Y. Cheng, Q. Gu, Z. Wang, Y. Shen, D. Yin, L. Wang and G. Huang, *Nanoscale*, **13**, 3808 (2021).